



**HAL**  
open science

# High-order polynomial approximations for solving non-inertial particle size density in flames

Luc Vervisch, Guido Lodato, Pascale Domingo

► **To cite this version:**

Luc Vervisch, Guido Lodato, Pascale Domingo. High-order polynomial approximations for solving non-inertial particle size density in flames. Proceedings of the Combustion Institute, In press, 10.1016/j.proci.2022.06.022 . hal-03784202

**HAL Id: hal-03784202**

**<https://normandie-univ.hal.science/hal-03784202>**

Submitted on 22 Sep 2022

**HAL** is a multi-disciplinary open access archive for the deposit and dissemination of scientific research documents, whether they are published or not. The documents may come from teaching and research institutions in France or abroad, or from public or private research centers.

L'archive ouverte pluridisciplinaire **HAL**, est destinée au dépôt et à la diffusion de documents scientifiques de niveau recherche, publiés ou non, émanant des établissements d'enseignement et de recherche français ou étrangers, des laboratoires publics ou privés.

## Proceedings of the Combustion Institute

### High-order polynomial approximations for solving non-inertial particle size density in flames

--Manuscript Draft--

<b>Manuscript Number:</b>	PROCI-D-22-00631R2
<b>Article Type:</b>	Vol. 39: 12: Numerical Combustion
<b>Section/Category:</b>	12: Numerical Combustion
<b>Keywords:</b>	Particle size distribution; Population balance equation; high-order approximations; Carbon particles simulation; Collision integral quadrature
<b>Corresponding Author:</b>	Luc vervisch, Dr INSA de Rouen Saint-Etienne-du-Rouvray, FRANCE
<b>First Author:</b>	Luc vervisch, Dr
<b>Order of Authors:</b>	Luc vervisch, Dr Guido Lodato, PhD Pascale Domingo, PhD
<b>Abstract:</b>	<p>A novel numerical framework is discussed to simulate the time evolution of non-inertial particle size distributions (or number density functions) in flames. The generic form of the population balance equation is considered featuring nucleation, surface growth/loss and agglomeration/coagulation. This balance equation is first recast in a form that is prone to minimize spurious numerical errors in the simulation of surface growth/loss and collision integrals. Formally, this is achieved classifying the terms of the equation into: (i) Lagrangian transport in size-space (surface growth/loss), (ii) relaxation rates of the particle density at a given size (non-uniform growth/loss and negative contribution of collision integrals) and (iii) sources (nucleation and positive contribution of collision integrals). To secure accuracy, a high-order modal decomposition of the particle size distribution is introduced within every section of size considered. A Legendre polynomials basis is used with Gauss-Lobatto quadrature points. By construction, the method performs very well for dealing with particle surface growth/loss and it is also highly accurate for the estimation of the collision integrals thanks to the high-order quadrature. This is confirmed simulating canonical test cases of the literature to compare the numerical results against exact and analytical solutions. With a discretisation based on about 40 sections of size and with Legendre interpolation at the 5th-order, very good accuracy is obtained up to the third moment of the distributions for particle size ranging over up to 8 orders of magnitude. The method is cast to minimize computing cost. Strategies to couple this novel numerical framework with the simulation of carbon particles dynamics in flames are discussed.</p>

# High-order polynomial approximations for solving non-inertial particle size density in flames

Luc Vervisch\*, Guido Lodato, Pascale Domingo

*CORIA-CNRS, INSA Rouen Normandie, Saint-Etienne-du-Rouvray, France*

June 10th, 2022

---

## Abstract

A novel numerical framework is discussed to simulate the time evolution of non-inertial particle size distributions (or number density functions) in flames. The generic form of the population balance equation is considered featuring nucleation, surface growth/loss and agglomeration/coagulation. This balance equation is first recast in a form that is prone to minimize spurious numerical errors in the simulation of surface growth/loss and collision integrals. Formally, this is achieved classifying the terms of the equation into: (i) Lagrangian transport in size-space (surface growth/loss), (ii) relaxation rates of the particle density at a given size (non-uniform growth/loss and negative contribution of collision integrals) and (iii) sources (nucleation and positive contribution of collision integrals). To secure accuracy, a high-order modal decomposition of the particle size distribution is introduced within every section of size considered. A Legendre polynomials basis is used with Gauss-Lobatto quadrature points. By construction, the method performs very well for dealing with particle surface growth/loss and it is also highly accurate for the estimation of the collision integrals thanks to the high-order quadrature. This is confirmed simulating canonical test cases of the literature to compare the numerical results against exact and analytical solutions. With a discretisation based on about 40 sections of size and with Legendre interpolation at the 5th-order, very good accuracy is obtained up to the third moment of the distributions for particle size ranging over up to 8 orders of magnitude. The method is cast to minimize computing cost. Strategies to couple this novel numerical framework with the simulation of carbon particles dynamics in flames are discussed.

*Keywords:* Particle size distribution; Population balance equation; high-order approximations; Carbon particles simulation; Collision integral quadrature

---

**Colloquium:** Numerical Combustion including discretization and meshing techniques, high-order methods, high performance computing, machine learning, uncertainty quantification, experimental design, and generation of numerical data.

\*corresponding author: luc.vervisch@insa-rouen.fr

## Nomenclature

$N$	Number of sections of size
$n_L$	Number of Gauss-Lobatto points
$p$	Order of interpolation
$v_j^i$	Particle size in the $i$ -th section at the $j$ -th interpolation point
$n(v_j^i, t)$	Particle size distribution (PSD)
$\xi_j$	Gauss-Lobatto interpolation points
$P_k(\xi_j)$	Legendre polynomial of order $k$
$\phi_k^i$	$k$ -th mode of the PSD in the $i$ -th section in the Legendre basis

## 1. Introduction

Accurately simulating the distribution of sizes of non-inertial particles is crucial to help in design and optimisation of many combustion applications, both in the quest of optimising combustion systems to mitigate particulate and soot emission and in the manufacture of carbon nanotubes, nanosilver and other advanced carbon-based materials (see [1] for a review).

In addition to the complexity of the thermophysical modeling of the gaseous and solid phases at play in nucleation, surface growth/loss, agglomeration/coagulation and sometimes breakage of the particles, serious numerical issues arise when solving the population balance equation (PBE) describing the dynamics of the particles size distribution (PSD). Non-linear convective effects in size-space due to growth/loss of the particle surface and agglomeration/coagulations/breakage processes are challenging to discretise and simulate over size ranges which can cover up to five or six orders of magnitude (i.e., from nanometer to millimetre).

Numerous approaches and numerical methods have been discussed and applied [2-11] and many references therein. The thermophysical models are usually developed by comparing their predictions against experimental results after solving the PBE. Thereby, to avoid calibrating these models while including numerical error compensation, accurate PBE solving methods are required. This is even more crucial with the emergence of neural networks trained to solve for PBE [12], thus allowing for applying more detailed physical descriptions to simulate complex systems at a reasonable CPU cost. The PBE solution database used for such training must be free from numerical artefact.

In this work we develop a strategy to solve for such non-inertial particles dynamics. First the time evolution of the particle size distribution is cast in a specific manner, which minimises the error in the solving of surface growth/loss. It relies on a characteristic-like treatment of the PSD in size-space, as in [13], associated here to a modal high-order approximation within sections of size, which allows to accurately locate the root of the characteristic. This modal high-order approximation goes with Gauss-Lobatto quadrature points, which also facilitate and improve the calculation of the collisions integrals. This fully new method

(at least to the best knowledge of the authors) is tested against analytical solutions to focus on numerical accuracy. Its combination with flow solution through a sectional method through neural networks training, is finally discussed.

## 2. PBE solving formulation

Let us denote the PSD (or the number density function)  $n(v; \underline{x}, t)$  as the number of particles of characteristic size  $v$  (in terms of volume or mass,  $v$  is a continuous independent variable), per unit of flow volume and per unit of characteristic size. The evolution of  $n(v; \underline{x}, t)$  follows the generic form of a population balance equation [14,15],

$$\frac{\partial \rho n(v; \underline{x}, t)}{\partial t} + \nabla \cdot (\rho \underline{u} n(v; \underline{x}, t)) = -\rho \frac{\partial}{\partial v} [G(v; \underline{x}, t) n(v; \underline{x}, t)] + \rho \dot{A}(v; \underline{x}, t), \quad (1)$$

with  $\rho$  the density,  $\underline{u}$  the flow velocity,  $G(v; \underline{x}, t)$  the particle surface growth/loss rate and

$$\begin{aligned} \dot{A}(v; \underline{x}, t) &= \dot{h}(v; \underline{x}, t) \\ &+ \frac{1}{2} \int_0^v \beta(v-v^*, v^*) n(v-v^*; \underline{x}, t) n(v^*; \underline{x}, t) dv^* \\ &- n(v; \underline{x}, t) \int_0^\infty \beta(v, v^*) n(v^*; \underline{x}, t) dv^*, \quad (2) \end{aligned}$$

where  $\dot{h}(v; \underline{x}, t)$  is the nucleation term and  $\beta(v, v^*)$  the collision kernel of two particles entering the so-called Smoluchowski integrals.

How to account for non-homogeneous mixtures in the proposed approach, in other words for  $\nabla \cdot (\rho \underline{u} n(v; \underline{x}, t))$ , is discussed thereafter. First, the evolution in size space is isolated (i.e., space is omitted the relations being valid for every points of a three-dimensional domain [1]) and the PBE is reorganised under the form:

$$\frac{\partial n(v; t)}{\partial t} + G(v; t) \frac{\partial n(v; t)}{\partial v} = -\dot{b}(v; t) n(v; t) + \dot{c}(v; t), \quad (3)$$

with

$$\dot{b}(v; t) = \frac{\partial G(v; t)}{\partial v} + \int_0^\infty \beta(v, v^*) n(v^*; t) dv^*, \quad (4)$$

and

$$\begin{aligned} \dot{c}(v; t) &= \dot{h}(v; t) \\ &+ \frac{1}{2} \int_0^v \beta(v-v^*, v^*) n(v-v^*; t) n(v^*; t) dv^*. \quad (5) \end{aligned}$$

<sup>1</sup>Flow continuity ( $\partial \rho / \partial t + \nabla \cdot (\rho \underline{u}) = 0$ ) is accounted for before setting  $\nabla n(v; \underline{x}, t) = 0$ .



Table 1: Position and weights of the Gauss-Lobatto quadrature points used for 5-th order interpolation.

$j$	$\xi_j$	$w_j$
$j = 0$	-1	1/15
$j = 1$	$-\sqrt{1/3 + 2\sqrt{7}/21}$	$(14 - \sqrt{7})/30$
$j = 2$	$-\sqrt{1/3 - 2\sqrt{7}/21}$	$(14 + \sqrt{7})/30$
$j = 3$	$\sqrt{1/3 - 2\sqrt{7}/21}$	$(14 + \sqrt{7})/30$
$j = 4$	$\sqrt{1/3 + 2\sqrt{7}/21}$	$(14 - \sqrt{7})/30$
$j = 5$	1	1/15

posed in the basis Legendre functions [18],  $P_k(\xi_j)$  used for interpolating the solution at  $\xi_j \in [-1, +1]$ , the  $n_L$  Gauss-Lobatto points within the section (Fig. 1). These points are defined so that  $\xi_j$  is the  $j$ -th zero of  $P'_k(\xi)$ , the derivative of the standard Legendre functions. The values of the  $\xi_j$  are given in Table 1 for the fifth-order approximation used in this study. The points within the  $i$ -th section are then distributed according to

$$v_j^i = \frac{\xi_j + 1}{2} (v_{n_L-1}^i - v_0^i) + v_0^i, \quad (16)$$

with  $v_{n_L-1}^i = v_0^{i+1}$ , because the Gauss-Lobatto points include the end points of the section. The modes are computed from  $[P_k(\xi_j)]^{-1}$  the inverse of the polynomial basis

$$\phi_k^i(t) = \sum_{j=0}^p [P_k(\xi_j)]^{-1} n(\xi_j(v_j^i); t). \quad (17)$$

In practice, the inverse of the matrix  $A_{kj} = P_k(\xi_j)$ , characterising the polynomial basis, is computed once for all. When needed, the  $\phi_k^i$  are computed from (17) and from (15),  $n(v; t)$  can be interpolated at high-order for any value of  $v$ .

To compute the collision integrals, the Gauss-Lobatto quadrature rule is used. The integral in the terms  $\hat{b}(v_j^i; t)$  (Eq. 4) then reads

$$\int_{v_0^0}^{v_{n_L-1}^{N-1}} \beta(v_j^i, v^*) n(v^*; t) dv^* = \sum_{k=0}^{N-1} \sum_{\ell=0}^{n_L-1} \beta(v_j^i, v_\ell^k) n(v_\ell^k; t) \gamma_{\ell k}, \quad (18)$$

where the weights of the quadrature are given by

$$\gamma_{\ell k} = w_\ell \left( \frac{v_{n_L-1}^k - v_0^k}{2} \right), \quad (19)$$

with  $w_0 = w_{n_L-1} = 2/(n_L(n_L - 1))$  and  $w_\ell = 2/(n_L(n_L - 1)[P'_{n_L-1}(\xi_\ell)]^2)$  for  $1 \leq \ell \leq n_L - 2$

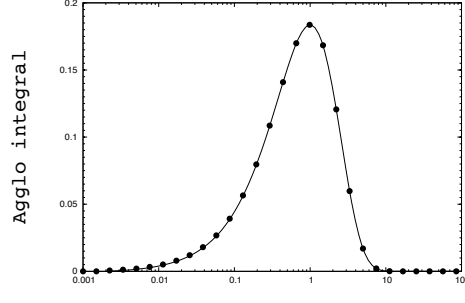


Fig. 2: Agglomeration term Eq. (5). Line: Analytical  $0.5(v - 2v_0) \exp(-v)$ . Circle: Computation by Eq. (20).

(see Table 1). Similarly, the integral in  $\hat{c}(v_j^i; t)$  reads

$$\int_{v_0^0}^{v_j^i - v_0^0} \beta(v_j^i - v^*, v^*) n(v_j^i - v^*; t) n(v^*; t) dv^* = \sum_{k=0}^i \sum_{\substack{\ell=0 \\ v_\ell^k \leq v_j^i - v_0^0}}^{n_L-1} \beta(v_j^i - v_\ell^k, v_\ell^k) n(v_j^i - v_\ell^k; t) n(v_\ell^k; t) \gamma_{\ell k} \quad (20)$$

where  $v_\ell^k$  is defined by Eq. (16), but for  $i = 0$ ,  $i = N - 1$  and  $k = i$ , i.e., when the  $v_\ell^k$  values cannot cover the entire of a section, the quadrature points must be re-organised over the interval left for integration within the section

$$v_\ell^k = \frac{\xi_\ell + 1}{2} (v_j^i - v_0^0 - v_0^i) + v_0^i. \quad (21)$$

The weights of the quadrature  $\gamma_{\ell k}$  (Eq. (19)) are then also rescaled according to the size-space covered in the concerned sub-section.

Because of the non-uniform distribution of the sections,  $v_j^i - v_\ell^k$  is likely to be located between two solution points, then in Eq. (20) the PSD amplitude is estimated from the high-order approximation using Eq. (15).

#### 4. Analytical test cases

Many canonical test cases exist in the literature to validate numerics dedicated to the solving of PBE [4, 19, 22]. A selection of the most challenging which provides analytical solutions to compare with are now used to evaluate the proposed method, thus isolating the potential numerical errors from physical modeling.

These problems are formulated in a dimensionless manner, the time-step is set to  $\delta t = 0.01$  and a fifth order interpolation is used ( $p = 5$ ,  $n_L = 6$ )

##### 4.1. Collision integrals

Table 2: Departure to the analytical solution in the prediction of the three first moments  $M_m = \int v^m n(v) dv$ . Cases Agg(a)-(b),  $t = 20$ . Cases Agg+G(a)-(b),  $t = 7$ . Sec: two-point sectional method (see Table 5 in [24]).

Case	Error %	Present	Sec
Agg(a)	$\epsilon_{M_1}$	0.4	0.4
	$\epsilon_{M_2}$	1.3	1.6
	$\epsilon_{M_3}$	11	–
Agg(b)	$\epsilon_{M_1}$	0.081	-1.1
	$\epsilon_{M_2}$	1.84	0.4
	$\epsilon_{M_3}$	5.89	–
Agg+G(a)	$\epsilon_{M_1}$	0.97	5.4
	$\epsilon_{M_2}$	1.55	48 783
	$\epsilon_{M_3}$	1.81	–
Agg+G(b)	$\epsilon_{M_1}$	1.31	5.4
	$\epsilon_{M_2}$	8.42	22 141
	$\epsilon_{M_3}$	16.81	–

A first stringent test is performed focussing on the calculation of the collision integrals. Numerical errors easily arise in the computation of these integrals, because they explicitly couple every characteristic size solved for the PSD with the full range of sizes considered [16, 23].

The numerical results are compared to the analytical solution of the collision integral present in  $\dot{c}(v; t)$  for the representative distribution  $n(v) = \exp(-v)$ , submitted to a size-free collision kernel  $\beta = 1 \forall v$ :

$$\frac{1}{2} \int_{v_o}^{v-v_o} \beta(v-v^*, v^*) n(v-v^*; t) n(v^*; t) dv^* = \frac{1}{2} (v-2v_o) \exp(-v) \quad (22)$$

Figure 2 shows the results over 5 decades using 40 sections distributed over a geometric grid

$$v_0^i = v_0^0 F_s^i, \quad (23)$$

with  $v_0^0 = 10^{-3}$  and  $F_s = 1.33$ . The collision integral is approximated with a precision that could hardly be reached without benefiting from the quadrature points within the sections. The same level of precision is obtained for the remaining collision term in  $\dot{b}(v; t)$ , which is easier to compute because it depends on size only through the collision kernel. As now shown, this will be instrumental in securing the accurate prediction of the PSD moments in an iterative process solving for the PBE.

#### 4.2. Agglomeration

Once the calculation of the collision integral verified, a pure agglomeration process is considered. Starting from an exponential distribution  $\exp(-v)$  discretized over an exponential grid [21]

$$v_0^i = 10^{-3} \left( 1 + \frac{1-\alpha^i}{1-\alpha} \right), \quad (24)$$

with  $\alpha = 1.17$  and with a size-space covering  $6.7 \cdot 10^{-2} < v < 200$  over 40 sections.

Considering first a fixed collision kernel  $\beta = 1$  (case Agg(a)), the analytical solution reads [19],

$$n(v; t) = \frac{4}{(t+2)^2} \exp\left(-\frac{2v}{t+2}\right). \quad (25)$$

Figure 3(a) compares this exact solution to the numerical one at time  $t = 10$  and  $t = 20$ , obtained using Eq. (14) with  $v^- = v$  ( $G = 0$ ). The PSD shape is very well captured confirming the precise estimation of the Smoluchowski integrals by [18] and [20]. The departure of the three first moments from their analytical counterpart is computed from [25] at time  $t = 20$  and given in % in Table 2. The errors are below those reported with 2pt and 3pt sectional methods [20] for the same test case [24], specifically for the third moment for which that level of accuracy has not been reached in former works. Additional tests decreasing the number of sections show that the errors increase at a much slower rate with the present method than with the sectional methods. The usual tradeoff between CPU cost and desired accuracy, going along with the introduction of high-order polynomial approximations, must thus be somehow managed when selecting the number of sections.

A non-uniform collision frequency with the Golovin sum kernel  $\beta(v, v^*) = v + v^*$ , featuring the increase with volume of the collision frequency between two particles of characteristic sizes  $v$  and  $v^*$ , is now considered as an additional pure agglomeration test (case Agg(b)). The exponential grid with 40 sections is also used, but here with  $\alpha = 1.25$ , leading to larger domain size  $6.7 \cdot 10^{-2} < v < 2000$ . Starting from the exponential distribution, the analytical solution of the PSD may be written [19]

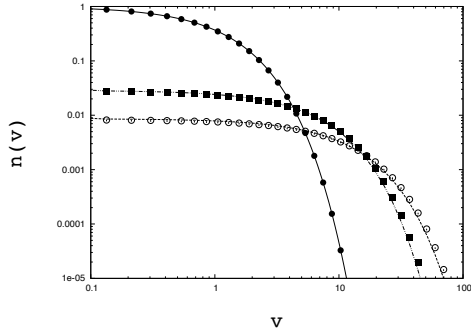
$$n(v; t) = \left( \frac{1-\theta}{\theta^{1/2}} \right) \frac{\exp(-v(\theta+1))}{v} I_1 \left[ 2v\theta^{1/2} \right], \quad (26)$$

with  $\theta = 1 - \exp(-t)$  and  $I_1$  the modified Bessel function of the first kind of order unity. The comparison between the analytical solution and the high-order solution can be seen in Fig. 3(b), the quality of the results is comparable to the one obtained with the fixed collision kernel, also in terms of the prediction of the moments (Table 2).

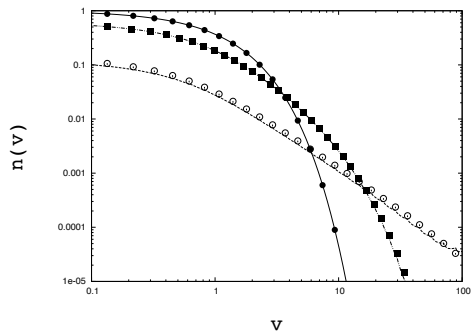
#### 4.3. Surface growth/loss

The basic test of pure surface growth/loss allows to verify that the PSD is transported in size space without any deformation. In Fig. 4 a representative hyperbolic tangent PSD featuring significant gradients is convected back and forth over a uniform grid of 50 sections covering a length of 4. The normalised surface growth/loss rate is  $G = 0.05$  for  $t < 40$  and  $G = -0.05$  for  $t > 40$ .

The particle size distributions in Fig. 4 shows that the characteristic-like approach (Eq. (8)), combined with high-order approximation, offers a noise-free



(a) Case Agg(a):  $\beta = 1$



(b) Case Agg(b):  $\beta(v, v^*) = v + v^*$

Fig. 3: PSD  $n(v, t)$ . Pure agglomeration cases Agg(a)-(b). Symbol: Analytical solution. Lines: High-order solution. Black circle and solid-line:  $t = 0$ . Square and dot-dash line:  $t = 10$ . Empty circle and dotted line:  $t = 20$

surface growth/loss simulation.  $n(v; t)$  returns to the exact same distribution after applying surface growth for  $t = 40$  and surface loss at the same rate for that same duration.

#### 4.4. Agglomeration and surface growth

Combining agglomeration with surface growth,  $G(v) = v$ , and starting from the exponential distribution, the time evolution of the PSD should follow the analytical solution [22]:

$$n(v; t) = \frac{4}{(2 + \beta_0 t)^2} \exp\left(-\frac{2v \exp(-t)}{2 + \beta_0 t} - t\right). \quad (27)$$

The size-independent collision kernel is set to  $\beta = 0.1$  (case Agg+G(a)) and to  $\beta = 1.0$  (case Agg+G(b)). A geometrical grid is used (Eq. (23)) with  $F_s = 1.7$ , to cover the size range  $10^{-5} < v < 1.6 \cdot 10^6$ . Results are presented in Fig. 5 in terms of  $n(v; t) \cdot v$ , both in linear and logarithmic scale for the distributions, to avoid the risk in concluding solely from log-plots for physical problems with a pronounced sensitivity to small fluctuations of size around a targeted peak level.

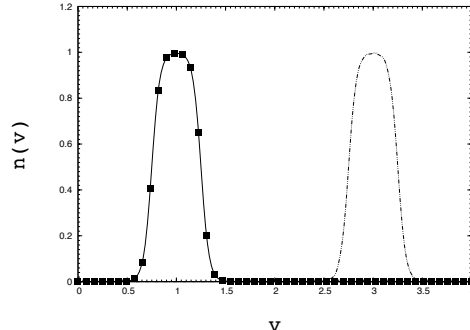


Fig. 4: Pure surface growth/loss. Line: Initial condition. Dashed dot:  $t = 40, G = 0.05$ . Square and dot-dash line:  $t = 80$  with  $G = -0.05$  for  $t > 40$ .

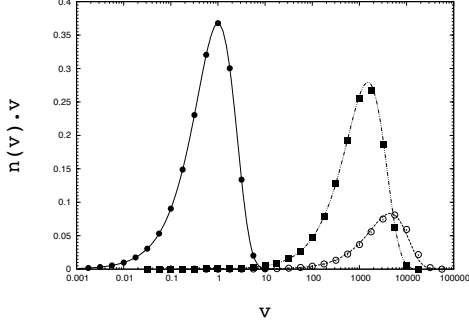
Both the time evolution of the amplitude of the PSD over all sizes (Fig. 5) and its moments at  $t = 7$  (Table 2) are well captured. Here one should notice that the error is much smaller than usually reported with sectional methods for this test case [24]. Errors of about 5% were found for the first moment with the same number of sections using 2- and 3-point sectional methods, however with the impossibility of predicting the second order moment, for which error raised up to more than 48 000% (see Table 2). The potential of formulating the solution as in Eq. (14) becomes then fully apparent.

Also, thanks to the simple characteristic formulation for simulating surface growth/loss and to the pre-computation of the matrix entering the calculating the modes of the Legendre decomposition (Eq. (17)), in the end, the number of operations is just 3% above the one required with usual 2-point sectional methods. Therefore, the cost in terms of CPU time stays similar to the one of much lower-order approximations, which did not take advantage of the time-evolution of the PSD formulated as in Eq. (14).

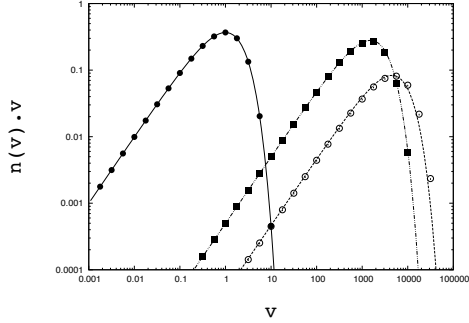
#### 4.5. Nucleation and surface growth

To further test the method, nucleation and surface growth are now combined. The source is given by  $h(v_0) = 1$  and surface growth by  $G(v) = v$ . The initial condition is a stiff hyperbolic tangent of amplitude  $10^{-5}$  and located at  $v_0$ . The amplitude of this initial distribution is five time smaller than the expected solutions for  $t > 0$ . As many other approaches solving for PSD, the present method cannot handle a distribution exactly set at zero at initial time, instead a vanishing distribution must be imposed, without impacting on the accuracy as seen thereafter. The grid is still geometrical (Eq. (23)) with  $F_s = 1.7$ .

Such a physical problem should lead to a uniform distribution progressing over size-space. This is what is indeed observed in Fig. 6. In previous works, more or less pronounced oscillations about the uniform distribution have been reported [20, 24]. Hence, the present approach allows for simulating nucleation and



(a) y-axis Linear



(b) y-axis Log

Fig. 5: PSD  $n(v, t) \cdot v$ . Case Agg+G: surface growth  $G(v) = v$  and agglomeration with size-free collision kernel  $\beta$ . Symbols: Analytical solution. Lines: high-order solution. Black-circle and solid-line:  $t = 0$ . At  $t = 7$ , square and dot-dash line: case Agg+G(a)  $\beta = 0.1$ . Empty circle and dash line: Agg+G(b)  $\beta = 1$ .

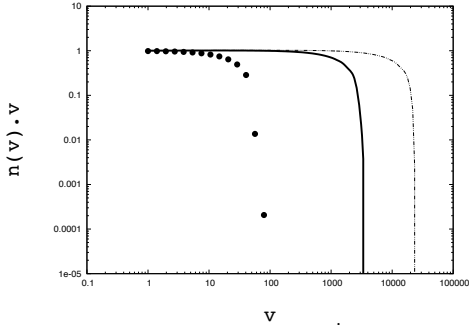


Fig. 6:  $n(v, t) \cdot v$ . Constant nucleation,  $\dot{h}(v_0) = 1$ , with surface growth  $G(v) = v$ . Circle:  $t = 4$ . Line:  $t = 8$ . Dashed-dot:  $t = 10$ .

growth without any spurious numerical noise (Fig. 6).

#### 4.5.1. Nucleation, surface growth and agglomeration

A final test case is applied to verify that the method can handle bi-modal distributions. The sur-

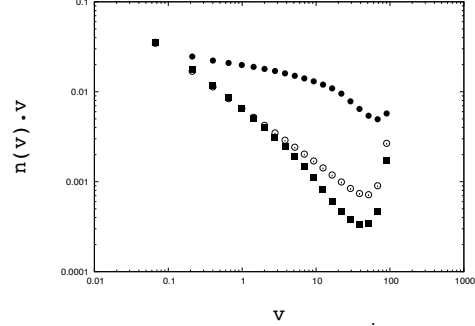


Fig. 7:  $n(v, t) \cdot v$ . Constant nucleation,  $\dot{h}(v_0) = 1$ , with surface growth,  $G(v) = 1.2v$ , and agglomeration,  $\beta(v, v^*) = 1.5(v+v^*)$ . Full circle:  $t = 5$ . Circle:  $t = 10$ . Square:  $t = 15$ .

face growth  $G(v) = 1.2v$ , the nucleation source  $\dot{h}(v_0) = 1$  and an agglomeration kernel  $\beta(v, v^*) = 1.5(v+v^*)$  are imposed. 40 sections are used with an exponential grid with  $\alpha = 1.15$  (Eq. 24). The initial condition is here again a stiff hyperbolic tangent of vanishing amplitude  $10^{-5}$  located at  $v_0$ .

As expected for these conditions, Fig. 7 shows a distribution evolving towards a bi-modal shape, with nucleation feeding the system with small particles to generate a first peak. Small particles which rapidly agglomerate and growth, to populate a second peak in the distribution of size.

## 5. Coupling with flow solution

The coupling of this PBE solving with flow solution can be achieved following different routes. First we must acknowledge that it would not be practical to transport with the flow all the solution points  $n(v_j^i; \underline{x}, t)$ .

The most advanced and CPU efficient approach would consist of adopting the strategy discussed in [12], in which PBE solutions are generated to train neural networks. Thereby replacing in this process former methods used to solve for the PBE by the present one, to generate databases for the training of a combination of artificial neural networks (ANN), convolutional neural networks (CNN) and recurrent long short-term memory artificial neural layers (LSTM) for the prediction of the PSD [12].

During the training phase of this machine learning approach, in every section, the average number of particles size per unit of flow volume can be easily computed from the quadrature points,

$$N^i(\underline{x}, t) = \int_{v_0^i}^{v_{n_L}^i-1} n(v; \underline{x}, t) dv = \frac{v_{n_L}^i-1 - v_0^i}{2} \sum_{\ell=0}^{n_L-1} n(v_\ell^i; \underline{x}, t) w_\ell. \quad (28)$$

These  $N^i(x, t)$  will be transported for convection and eventually diffusion in the flow solver, as it would be the case for any sectional method, whereas the evolution in size-space is handled by the networks thanks to two set of neurons: Firstly, an ANN takes as inputs the thermophysical parameters controlling  $G(v; \underline{x}, t)$  and  $\dot{A}(v; \underline{x}, t)$  and the time step. Secondly, collecting the  $N^i(x, t)$  for  $i \in [0, N - 1]$  constitutes a one-dimensional ‘image’ which is handled by a CNN. From these inputs, the ANN-CNN is trained to return the PSD shape for the subsequent time step.

Such strategy was demonstrated already for laminar sooting flames [12]. In this former work, it was shown how, for a fixed network architecture and thus fixed CPU cost, the increase of the precision of the training database benefited to the subsequent prediction by the networks. The method proposed in this work could be very useful along these lines.

Because of the high Schmidt number character of soot, the recently developed numerical method to secure the sub-grid scale flow transport of high Schmidt number scalars, could complement the methodology [25].

## 6. Conclusion

In the development of numerical tools for predicting carbon-based material derived from processes involving combustion and flames, the use of numerically precise methods is mandatory to alleviate error compensation between the modeling of the thermophysics and the numerics. Along these lines, a novel formalism has been proposed to cast the time discretisation of the population balance equation, which controls the time evolution of particle size distributions, into a form that is further combined with a high-order approximation of these distributions within sections of size.

The surface growth/loss is handled through a characteristic-like propagation of the particle size distribution. The Smoluchowski collision integrals are accurately computed thanks to Gauss-Lobatto quadrature points, introduced with the Legendre polynomial basis providing a high-order approximation of the distribution of sizes.

Because of the specific form retained for the time-advancement of the population balance equation, the CPU cost stays moderate and the coupling with usual flow solvers can be envisioned easily and a strategy to do so has been discussed.

The method has been carefully tested with success against analytical solutions including surface growth/loss, agglomeration and nucleation. This was done for representative distributions covering up to 8 order of magnitudes in size space, with an accurate prediction up to the third moment.

A perspective lies in the possibility of incorporating additional information within the particle size distribution to improve the representation of carbon particles in flames. Indeed, a multivariate description can easily be envisioned considering a polynomial

basis for every variable introduced to control joint-distributions, as usually done for instance in multi-dimensional high-order flow solution [26].

## References

- [1] G. A. Kelesidis, E. Goudeli, and S. E. Pratsinis. Flame synthesis of functional nanostructured materials and devices: Surface growth and aggregation. *Proc. Combust. Inst.*, 36(1):29–50, 2017.
- [2] S. Rigopoulos. Modelling of soot aerosol dynamics in turbulent flow. *Flow Turbulence Combust.*, 103:565–604, 2019.
- [3] D. L. Marchisio and R. O. Fox, editors. *Multiphase reacting flows: Modelling and simulation*, volume 492 of *CISM International Center for Mechanical Sciences*. Springer-Verlag, Wien, 2007.
- [4] F. Sewerin and S. Rigopoulos. An explicit adaptive grid approach for the numerical solution of the population balance equation. *Chemical Engineering Science*, 168:250 – 270, 2017.
- [5] R. Irizarry. Fast Monte Carlo methodology for multivariate particulate systems-I: Point ensemble Monte Carlo. *Chemical Engineering Science*, 63:95–110, 2008.
- [6] R. Irizarry. Fast Monte Carlo methodology for multivariate particulate systems-II:  $\tau$ -PEMC. *Chemical Engineering Science*, 63:111–121, 2008.
- [7] A. Attili and F. Bisetti. Application of a robust and efficient lagrangian particle scheme to soot transport in turbulent flames. *Comput. Fluids*, 84:164–175, 2013.
- [8] M. Singh, H. Y. Ismail, T. Matsoukas, A. B. Albadarin, and G. Walker. Mass-based finite volume scheme for aggregation, growth and nucleation population balance equation. *Proc. R. Soc. A*, 475:20190552, 2019.
- [9] S. Salenbauch, C. Hasse, M. Vanni, and D. L. Marchisio. A numerically robust method of moments with number density function reconstruction and its application to soot formation, growth and oxidation. *J. Aerosol Sci.*, 128:34–49, 2019.
- [10] A. Boje, J. Akroyd, S. Sutcliffe, and M. Kraft. Study of industrial titania synthesis using a hybrid particle-number and detailed particle model. *Chemical Engineering Science*, 219:115615, 2020.
- [11] A. Bouaniche, J. Yon, P. Domingo, and L. Vervisch. Analysis of the soot particle size distribution in a laminar premixed flame: A hybrid stochastic/fixed-sectional approach. *Flow Turbulence and Combust.*, 104:753–775, 2020.
- [12] A. Seltz, P. Domingo, and L. Vervisch. Solving the population balance equation for non-inertial particles dynamics using pdf and neural networks: Application to a sooting flame. *Phys. Fluids.*, 33(013311), 2021.

- [13] S. Kumar and D. Ramkrishna. On the solution of population balance equations by discretisation– III. Nucleation, growth and aggregation of particles. *Chem. Eng. Sci.*, 52(24):4659–4679, 1997.
- [14] D. Ramkrishna. *Population balances. Theory and applications to particulate systems in engineering*. Academic Press San Diego, 2000.
- [15] J. Solsvik and H. A. Jakobsen. The foundation of the population balance equation: A review. *Journal of Dispersion Science and Technology*, 36(4):510–520, 2015.
- [16] A. Liu and S. Rigopoulos. A conservative method for numerical solution of the population balance equation, and application to soot formation. *Combust. Flame*, 205:506–521, 2019.
- [17] Jan S. Hesthaven and Tim Warburton. *Nodal Discontinuous Galerkin Methods: Algorithms, Analysis, and Applications*. Springer Science & Business Media, LLC, 2008.
- [18] M. Abramowitz and I. A. Stegun. *Handbook of mathematical functions*. Dover, New York, 1970.
- [19] William T. Scott. Analytic studies of cloud droplet coalescence I. *Journal of the Atmospheric Sciences*, 25(1):54–65, 1968.
- [20] S.H. Park and S.N. Rogak. A novel fixed-sectional model for the formation and growth of aerosol agglomerates. *Journal of Aerosol Science*, 35(11):1385 – 1404, 2004.
- [21] S. Rigopoulos and A. G. Jones. Finite-element scheme for solution of the dynamic population balance equation. *AIChE Journal*, 49:1127 – 1139, 05 2003.
- [22] T. E. Ramabhadran, T. W. Peterson, and J. H. Seinfeld. Dynamics of aerosol coagulation and condensation. *AIChE Journal*, 22(5):840–851, 1976.
- [23] I. Pesmazoglou, A. M. Kempf, and S. Navarro-Martinez. Stochastic modelling of particle aggregation. *International Journal of Multiphase Flow*, 80:118 – 130, 2016.
- [24] A. Bouaniche, L. Vervisch, and P. Domingo. A hybrid stochastic/fixed-sectional method for solving the population balance equation. *Chem. Eng. Sci.*, 209:115198, 2019.
- [25] M. Leer, M. W. A. Pettit, J. T. Lipkowitz, P. Domingo, L. Vervisch, and A. M. Kempf. A conservative euler-lagrange decomposition principle for the solution of multi-scale flow problems at high schmidt or prandtl numbers. *J. Comput. Phys.*, 464(111216), 2022.
- [26] C. Liang, A. Jameson, and Z.J. Wang. Spectral difference method for compressible flow on unstructured grids with mixed elements. *J. Comput. Phys.*, 228(8):2847–2858, 2009.